ACS OMEGA

http://pubs.acs.org/journal/acsodf

Article

Development of a Radiotracer for PET Imaging of the SNAP Tag

Xinling Li,[⊥] Xiaochun Yang,[⊥] Zhijian Li,[⊥] Xiaobin Zheng, Yong-jian Peng, Wenjie Lin, Ling Zhou, Dehai Cao, Minyi Situ, Qingqiang Tu, Huiqiang Huang, Wei Fan,* Guokai Feng,* and Xiaofei Zhang*

Cite This: *ACS Omega* 2022, 7, 7550−7555

Read Online

ACCESS | Metrics & More | Article Recommendations | Supporting Information

ABSTRACT: Cell therapies have progressed to cures for hematopoietic disorders, neurodegenerative diseases, and cancer. However, only some patients can benefit from cell therapies even with prior screening. Due to the limited clinical methods to monitor the in vivo therapeutic functions of these transferred cells over time, the uncertain prognosis is hard to attenuate. Positron emission tomography (PET) cell tracking can provide comprehensive dynamic and spatial information on the proliferation status and whole-body distribution of the therapeutic cell. In this work, we designed and synthesized the first SNAP-tagged PET radiotracer. SNAP tag is an O^6-alkylguanine-DNA alkyltransferase that can form an irreversible bond with ^{18}F-BG-surface for in vivo cell tracking based on a reporter gene system. ^{18}F-BG-surface was obtained by the F-Al radiolabeling method in 32 ± 7% radiochemical yield and showed a high in vitro stability in mouse serum. SNAP-tagged cells could be selectively targeted by ^{18}F-BG-surface both in vitro (4.81 ± 0.08%AD/10^6 cell vs 2.26 ± 0.10%AD/10^6 cell) and in vivo (1.90 ± 0.05 vs 0.55 ± 0.02% ID/g, $p < 0.01$).

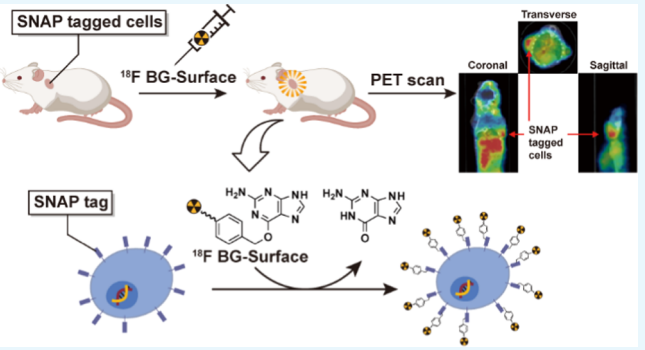

INTRODUCTION

In the past few decades, cell therapies have provided a promising way to treat various diseases.[1−3] Stem cell therapies and T-cell transfer therapies have progressed to the market or clinical trials for hematopoietic disorders, neurodegenerative diseases, and cancer.[4−6] However, only some patients can benefit from cell therapies even with prior screening. Moreover, toxicities, especially cytokine release syndrome (CRS) and immune effector cell-associated neurotoxicity syndrome (ICANS), of T-cell transfer therapies are difficult to predict.[7−11] This uncertainty in prognosis is hard to attenuate because of the limited clinical methods to monitor the in vivo therapeutic functions of these transferred cells over time. Positron emission tomography (PET) cell tracking can provide comprehensive dynamic and spatial information about the therapeutic cell proliferation status and whole-body distribution that blood samples or biopsies cannot and therefore can serve as a potent method for evaluation of cell therapy and response prediction.[12,13]

Depending on the labeling method, cell tracking with PET can be divided into indirect and direct labeling methodologies.[14−17] Indirect labeling takes advantage of genetically modified therapeutic cells. Cells transfected with a vector that contains a reporter gene express the reporter tag, which can be targeted by PET imaging probes. Reporter genes do not decrease or disappear with cell division, allowing continuous longitudinal imaging of cell tracking.[18,19] At present, reporters including herpes simplex virus type 1 thymidine kinase (HSV1-tk), hmTK2, hSSTr2, D2R, NIS, and hNET are used in PET cell imaging.[18,20−22] HSV1-tk and its mutant HSV1-sr39tk have been used to track cells in many clinical studies.[23,24] However, HSV1-tk and HSV1-sr39tk are both viral-derived, and the immunogenicity can be detrimental to the transferred cells. Although naturally expressed reporter genes such as human sodium iodide symporter, deoxycytidine kinase-based reporter gene, and human norepinephrine transporter (hNET) can avoid immunogenicity, their physiological expression hinders the success of clinical translation.[21,22] Human-derived reporter genes with little influence on endogenous expression have yet to be discovered.

The SNAP tag is an engineered mutant of the human repair protein O^6-alkylguanine-DNA alkyltransferase (hAGT), which can specifically form a stable covalent thioether bond with O^6-modified benzylguanine (BG) derivatives, thereby mediating the covalent labeling of the protein of interest (Figure 1). The human-derived SNAP tag is only 20 kDa, has little effect on the function of the target protein, and has been applied to the in vivo study of protein functions and the in vivo optical imaging of live cell tracking.[25,26]

Received: October 19, 2021
Accepted: February 1, 2022
Published: February 23, 2022

https://doi.org/10.1021/acsomega.1c05856
ACS Omega 2022, 7, 7550−7555

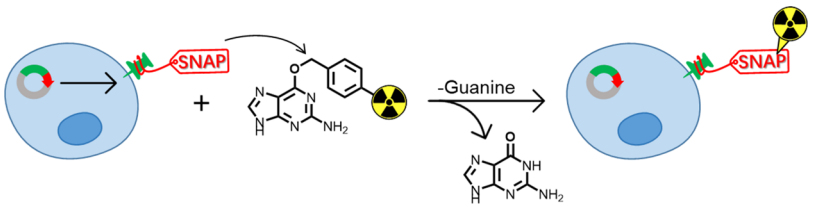

Figure 1. General mechanism of cell tracking with SNAP tag.

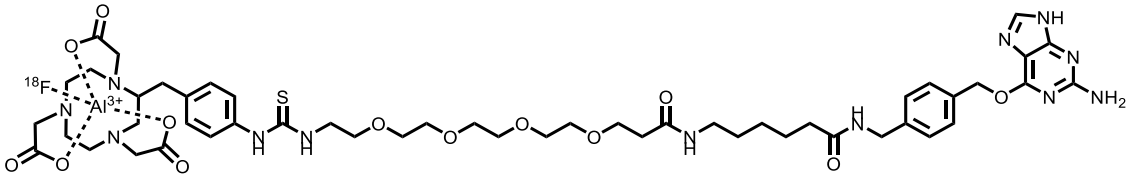

Figure 2. Chemical structure of BG-surface-PEG4-SCN-Bn-NOTA-Al^{18}F (^{18}F-BG-surface).

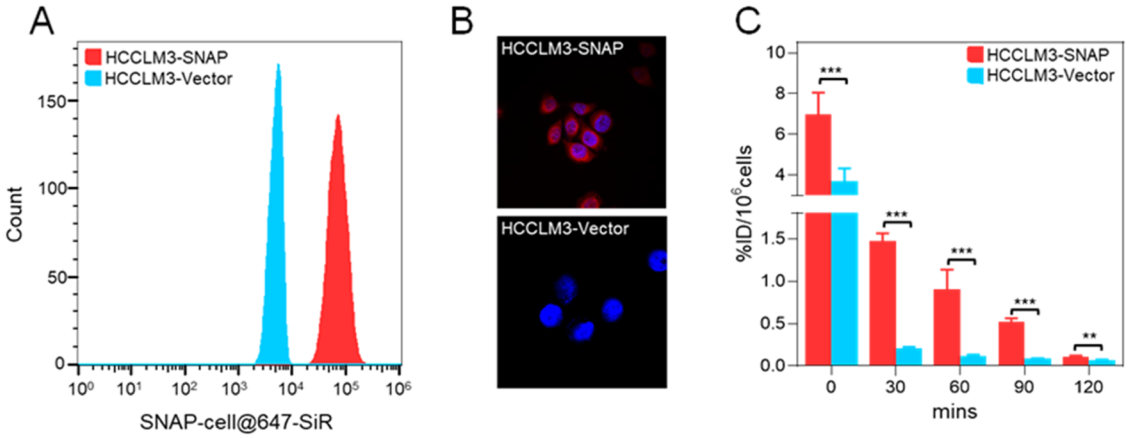

Figure 3. In vitro binding of HCCLM3-SNAP cells and BG tracer. (A) The binding of SNAP-cell@647-SiR and HCCLM3-SNAP cells was higher than the control cells. (B) Confocal imaging analysis of BG and HCCLM3-SNAP cells. The nucleus was stained with DAPI. HCCLM3-SNAP and its control cells were stained with SNAP-cell@647-SiR. DAPI was detected by a blue channel fluorescent dye, and SNAP-cell@647-SiR was detected by a red channel. (C) Quantification of ^{18}F-BG-surface cell retention. The tracer cell uptake was calculated as %AD/10^6 cell. HCCLM3-SNAP showed a significantly higher uptake than control cells. The statistical analysis was performed using Student's *t*-test, $n = 3$, $^{***}p < 0.01$.

Recently, a SNAP-tagged PET radiotracer, [^{18}F]FTBG, has been reported. [^{18}F]FTBG enabled in vivo targeting imaging of SNAP-tag$^+$ with the ratio of SNAP-tag$^+$ tumor/SNAP-tag$^-$ tumor being 2.5.[27] Herein, we report a new SNAP-tagged PET probe, ^{18}F-BG-surface. ^{18}F-BG-surface featured a PEG linkage and a NOTA ligand. ^{18}F-BG-surface showed good in vivo specific targeting toward the HCCLM3-SNAP cell in PET mice imaging with HCCLM3-SNAP/HCCLM3-Vector = 3.4.

RESULTS AND DISCUSSION

Based on the BG scaffold, we first designed a SNAP tag substrate precursor (BG-surface-PEG4-p-SCN-Bn-NOTA) (Figure S1) eligible for ^{18}F-Al labeling. We used ^{18}F as a radioactive probe because of its appropriate half-life and easy availability. The most applied ^{18}F labeling method is though the nucleophilic attack of anhydrous ^{18}F$^-$ to labeling precursors under heated conditions. However, nucleophilic ^{18}F labeling methods in dry solvents with a phase-transfer catalyst were tried, but no product was obtained. We suspect that BG derivatives were not stable in these labeling conditions. The alternative ^{18}F-Al radiolabeling method takes advantage of strong F−Al bonds and metal complexation reactions under acidic conditions to avoid deterioration of the precursor during labeling.[28−30] Our radiolabeled BG precursor featuring a chelating group of 1,4,7-triazacyclononanetr-iacetic acid (NOTA) linked with the BG core by a PEG linker was obtained by a three-step formal synthesis. BG-surface-PEG4-p-SCN-Bn-NOTA −AlF-^{18}F (known as ^{18}F-BG-surface in short) was obtained by labeling the precursor with ^{18}F$^-$ ions in the presence of Al^{3+} (Figure 2). The radiochemical yield of ^{18}F-BG-surface was approximately 32 ± 7% (non-decay-corrected, $n = 4$). The radiochemical purity of ^{18}F-BG-surface was >95%. The specific activity was 512 MBq/μmol, calculated on the starting amount of the SNAP tag substrate precursor (BG-surface). ^{18}F-BG-Surface was dried in vacuo and then reformulated in a saline solution at the end of the synthesis.

To evaluate the in vitro stability of ^{18}F-BG-surface, we incubated ^{18}F-BG-surface in mouse serum at 37 °C. After 30, 60, and 90 min, the radiochemical purity was determined by high-performance liquid chromatography (HPLC). As shown in Figure S3, the fraction corresponding to the intact ^{18}F-BG-surface remained unchanged, and no radio-metabolite was observed, indicating the excellent stability of ^{18}F-BG-surface during this time period and suggesting that this molecule could be used as a radioactive tracer for PET cell tracking.

To evaluate the in vitro binding effectiveness of the radiotracer ^{18}F-BG-surface, we stably transduced human

https://doi.org/10.1021/acsomega.1c05856
ACS Omega 2022, 7, 7550−7555

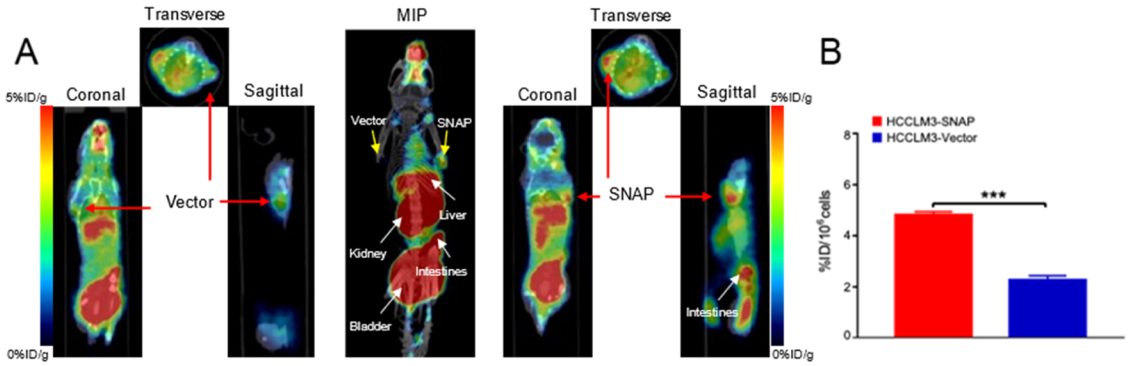

Figure 4. In vivo PET/CT imaging of HCCLM3 cell injection. (A) PET/CT of BALB/c nude mice injected with HCCLM3-SNAP cells and vector cells in the shoulder (yellow arrow). (B) Quantitative analysis of PET images. Volumes of interest (VOIs) were selected and calculated with PMOD image processing software. Data are %ID/g ± SD. Data are from five independent experiments. The statistical analysis was performed using Student's *t*-test, $n = 5$, $^{***}p < 0.01$.

hepatocarcinoma cells (HCCLM3) with SNAP-GPI, which has been reported to primarily localize to the cellular membrane. We chose transduced HCCLM3 to simulate the cell to track because of the convenience of immortality and the conception that the difference between different cell lines has limited influence on the binding function of the extramembrane anchored SNAP-GPI tag. Flow cytometry showed that the SNAP reporter gene-transduced cells (HCCLM3-SNAP) and the control cells (HCCLM3-Vector) were clearly divided into groups (Figure 3A). Both cell lines were stained with SNAP-cell@647-SiR, a commercially available fluorescent SNAP labeling substrate, and DAPI. Confocal fluorescence microscopy was used to confirm the expression of the SNAP tag. Clear fluorescence was observed on the cellular membrane of HCCLM3-SNAP cells, which was consistent with SNAP-GPI localization.

We next tested the ability of the radioactive tracer ^{18}F-BG-surface to label SNAP-tagged cells in vitro. ^{18}F-BG-surface was added to HCCLM3-SNAP and HCCLM3-Vector cells and coincubated for 0−120 mins before removing the unbonded ^{18}F-BG-surface by PBS washing. The radioactivity uptakes were quantified with a γ counter and calculated as the percentage of total added dose per 10^6 cells (%AD/10^6 cell). HCCLM3-Vector cells showed a significantly quicker radioactivity wash-out than HCCLM3-SNAP cells, which indicated a selective binding of ^{18}F-BG-surface and SNAP tag on the cell membrane. The time-dependent decreasing radioactivity of HCCLM3-SNAP cells may be due to the metabolism of SNAP-tagged GPI-induced irreversible consumption of ^{18}F-BG-surface.[31] The uptake ratio was the largest at 60 mins post administration (HCCLM3-Vector vs HCCLM3-Vector = 7.5) with average uptakes of 0.91 ± 0.23 and 0.12 ± 0.01%AD/10^6 cells, respectively.

A blocking study further showed that the uptake of ^{18}F-BG-surface in the SNAP-transduced cells could be blocked with a 1000-fold excess of BG-surface ($p < 0.05$). These results demonstrated the binding specificity of ^{18}F-BG-surface to the SNAP tag (Figure S4).

To study the pharmacokinetic property of ^{18}F-BG-surface, the distribution of ^{18}F-BG-surface in mice was studied. The results are expressed as the percentage of the injected dose per gram of tissue (% ID/g) in Figure S5B. High uptake (>3% ID/g) was observed in the liver and intestine at 1 h after injection of ^{18}F-BG-surface. The radioactivity levels in most tissues decreased 2 h post injection, while the signals remained high in the liver and intestine, which indicated hepatobiliary extraction as well as a possible intestinal reuptake pathway. This biodistribution of ^{18}F-BG-surface is in line with the previous report.[32] The slight increase of ^{18}F bone deposition at 2 h may result from the defluorination of ^{18}F-BG-surface though no apparent ^{18}F signal in the bones was observed with PET scan.[33]

PET imaging studies were performed to explore the in vivo cell tracing ability of ^{18}F-BG-surface with cell xenotransplantation mice, which were used in previous works for evaluation of the T-cell tracking probe.[18,34] Next, 1×10^6 HCCLM3-SNAP and HCCLM3-Vector cells were injected into the bilateral shoulder of the mice before ^{18}F-BG-surface was immediately injected into the mice through the tail vein. PET images were obtained 1 h after injection of the ^{18}F-BG-surface. PET images showed that the tracer accumulated in the subcutaneously injected HCCLM3-SNAP cells but accumulated less in the HCCLM3-Vector cells (1.90 ± 0.05 vs 0.55 ± 0.02%ID/g, $n = 5$, $p < 0.01$) (Figure 4). These results showed that PET imaging with ^{18}F-BG-surface was sensitive enough for the detection of SNAP-expressing cells (1×10^6), which is similar to the T-cell imaging threshold reported in the literature.[18,19] A tumor model was also established to evaluate the tracking ability of ^{18}F-BG-surface. ^{18}F-BG-Surface can still specifically bind to HCCLM3-SNAP after the tagged cell proliferation in vivo (Figure S6).

Conclusions. We have developed a new radiotracer ^{18}F-BG-surface based on the SNAP reporter system. In vitro stability and binding experiments showed that ^{18}F-BG-surface had a high selectivity toward SNAP-GPI-expressing cells and good metabolic stability. The subsequent PET imaging studies demonstrated that ^{18}F-BG-surface exhibited excellent in vivo selectivity. The subsequent PET imaging studies demonstrated that ^{18}F-BG-surface exhibited excellent in vivo selectivity. However, the high uptake in the liver and intestine could hinder the imaging. The pharmacokinetic property will be improved next before further exploring the application of the SNAP reporter gene in PET cell tracking and cell therapy.

MATERIALS AND METHODS

Cell and Mice. Hepatocellular carcinoma cell line HCCLM3 cells were purchased from the American Type Culture Collection (ATCC). The cells were cultured in the Dulbecco's Modified Eagle Medium (DMEM) medium containing 10% fetal bovine serum (FBS), and the cells were

https://doi.org/10.1021/acsomega.1c05856
ACS Omega 2022, 7, 7550−7555

maintained in an incubator with a humid atmosphere of 5% CO2 at 37 °C. We constructed a stable HCCLM3 cell line with the overexpression of SNAP. Animal experiments were approved by the Institutional Animal Care and Use Committee of Sun Yat-sen University Cancer Center. BALB/c nude mice used in the experiment were purchased from Charles River Life River, China (Beijing, China). The human SNAP gene was cloned, the recombinant retrovirus vector containing and not containing the SNAP gene was constructed, and the HCCLM3 transfection cell line expressing SNAP molecules (HCCLM3-SNAP) and their control groups (HCCLM3-Vector) was selected.

Immunofluorescence Staining. Approximately 2×10^4 HCCLM3-SNAP and HCCLM3-Vector cells were plated on coverslips separately with 200 μL of DMEM medium of 10% FBS. The cells on coverslips were coincubated with SNAP-cell@647-SiR (5 μg/μL) for 4 h at 37 °C after the cells grow to the logarithmic phase and then washed with PBS three times. The cells were fixed with 4% paraformaldehyde for 20 min and blocked in 5% bovine serum albumin (BSA) at room temperature for 1 h without light and then washed three times. The samples were incubated with 1 μg/mL 2-(4-amidinophenyl)-6-indolecarbamidine dihydrochloride (DAPI) (Beyotime, P0131, China) for 5 min in the dark and washed three times. The coverslips were mounted in ProLong Gold antifade (Invitrogen P26930). Fluorescence images were visualized and captured by a confocal microscopy confocal laser-scanning system (Olympus FV1000, Japan) at 60× and 120× magnification and analyzed using FluoView application software FV10-ASW 3.0. All assays were repeated at least three times.

Flow Cytometry Analysis. A total of 5×10^5 HCCLM3-SNAP and HCCLM3-Vector cells were added into 200 μL of DMEM medium with 10% FBS separately. The cells were added with 0.25 mM SNAP-Surface Alexa Fluor 647 (Abcam, ab272190), washed with PBS three times after a 1 h incubation at 37 °C, and resuspended with 500 μL of saline, and then, the expression of SNAP on the cell surface was detected. Flow cytometry acquisition was performed on a BD FacsCalibur (BD Bioscience). Analysis was performed using FlowJo software (Treestar). All assays were repeated at least three times.

In Vivo Metabolic Study. ^{18}F-BG-surface (100 μCi in 150 μL saline) was injected intravenously into mice, and the blood samples were collected after circulating 30 min for 1 and 2 h. The plasma was separated and analyzed by high-performance liquid chromatography (HPLC).

Synthesis of SNAP Tag Substrate Precursor (BG-Surface-PEG4-p-SCN-Bn-NOTA). The compound was prepared by Fmoc solid-phase peptide synthesis (SPPS). The Fmoc protecting group can ensure only reaction with BG under acidic conditions, and then, the Fmoc protecting group was deleted under alkaline conditions to link the C-terminus of PEG4 with p-SCN-Bn-NOTA (the synthetic route is shown above) (Figure S2). The final product was characterized with ^{1}H nuclear magnetic resonance spectra (H NMR), ^{13}C nuclear magnetic resonance spectra (C NMR), and high-resolution mass spectrometry (HRMS). H NMR were obtained at 600 MHz on Bruker spectrometers. ^{13}C NMR spectra were obtained at 151 MHz. Chemical shifts (δ) are reported in ppm, and coupling constants are reported in hertz. The multiplicities are abbreviated as follows: s, singlet; d, doublet; t, triplet; q, quartet; quint, quintet; sext, sextet; sept, septet; m, multiplet; br, broad signal; dd, doublet of doublets. For all of the HRMS measurements, the ionization method is ESI and the mass analyzer type is TOF on an AB SCIEX 500R mass spectrometer system. ^{1}H NMR (600 MHz, DMSO-d_6) δ 8.38 (s, 1H), 7.90 (s, 1H), 7.83 (s, 1H), 7.46 (s, 1H), 7.45 (s, 1H), 7.38 (s, 1H), 7.36 (s, 1H), 7.26 (s, 1H), 7.25 (s, 1H), 7.15 (s, 2H), 6.28 (s, 2H), 5.45 (s, 2H), 4.25 (d, J = 5.9 Hz, 2H), 3.62 (s, 3H), 3.57 (t, J = 6.5 Hz, 3H), 3.56 − 3.51 (m, 8H), 3.50 (s, 6H), 3.49−3.44 (m, 9H), 3.01 (q, J = 6.7 Hz, 3H), 2.29 (t, J = 6.5 Hz, 2H), 2.12 (t, J = 7.5 Hz, 2H), 1.51 (p, J = 7.5 Hz, 2H), 1.38 (p, J = 7.2 Hz, 2H), 1.24 (p, 2H). ^{13}C NMR (151 MHz, DMSO-d_6) δ 180.37, 173.56, 172.06, 171.25, 169.80, 169.15, 159.61, 139.63, 137.51, 135.16, 129.14, 128.56, 127.24, 122.75, 69.79, 69.75, 69.67, 69.58, 69.49, 68.52, 66.88, 66.52, 43.47, 41.78, 38.35, 36.13, 35.28, 28.89, 26.13, 25.05. HRMS (ESI): calculated for $C_{50}H_{73}N_{12}O_{13}S$[M + H], 1081.5141; found 1081.5138.

Radiolabeling of ^{18}F-BG-Surface. Freeze-dried powder of the SNAP tag substrate precursor (BG-surface) of weight 50 μg was dissolved with the addition of 60 μL of sodium acetate, 180 μL of ethanol, 10 μL of $AlCl_3$ (1 mM), and 74 MBq fluoride ion (approximately 2 mCi), and the mixture was boiled for 15 min at 100 °C and cooled down to room temperature. The ^{18}F-BG-surface product was captured using the C18 plus column (Waters, Sep-Pak), and the free fluoride ions would be filtered. The bound product on the C18 plus column was eluted with 400 μL of 70% ethanol after washing the C18 plus column with normal saline once; then, the solvent was evaporated in a vacuum before 150 μL of saline was added after measuring the radioactivity of ^{18}F-BG-surface for further usage.

In Vitro Uptake of Radiolabeled Probes in Cells Transduced with the SNAP Reporter Gene. A total of 1×10^6 HCCLM3-SNAP and HCCLM3-Vector cells were added into 200 μL of PBS separately. The cells were incubated with ∼370 kBq ^{18}F-BG-surface at 37 °C for 1 h before washed with 1 mL of cold PBS three times. The cells were resuspended with 500 μL of saline and recounted once, and then, the expression of SNAP on the cell surface was detected. The binding rates of two samples and BG were detected using the γ counter. All assays were repeated at least three times.

Whole-Body Ex Vivo Biodistribution of ^{18}F-BG-Surface. A total of 3.7 MBq (100 μCi) of ^{18}F-BG-surface was intravenously injected into each mouse. Four mice were sacrificed by cervical dislocation at each time point (60 min and 120 min). Major organs, heart, liver, spleen, lung, kidney, brain, intestine, bone, muscle, and blood were quickly collected and weighed. The radioactivity remaining in these organs was measured by a 2480 Wizard autogamma counter (PerkinElmer). The results are expressed as the percentage of injected dose per gram of wet tissue (% ID/g). All radioactivity calculations were decay-corrected based on the half-life of ^{18}F.

PET/CT Imaging of Cell Tracking Studies. A total of 1×10^6 SNAP-transduced and nontranduced cells were injected into the bilateral shoulder and back of mice separately (HCCLM3-SNAP was on the right side). Mice were anesthetized with 2.5% 10 μL/g tribromoethanol (T48402, Sigma, Aldrich, Germany) and injected intravenously with about ∼3.7 MBq (∼100 μCi) of ^{18}F-BG-surface. PET/CT scan was performed after ^{18}F-BG-surface was circulated in vivo for 1 h.

https://doi.org/10.1021/acsomega.1c05856
ACS Omega 2022, 7, 7550−7555

■ ASSOCIATED CONTENT

Supporting Information

The Supporting Information is available free of charge at https://pubs.acs.org/doi/10.1021/acsomega.1c05856.

Chemical structure of BG-surface-PEG4-p-SCN-Bn-NOTA; synthesis procedure of BG-surface-PEG4-p-SCN-Bn-NOTA; serum stability assay of ^{18}F-BG-surface; competitive inhibition of 18F-BG-surface and SNAP-transduced cells by BG-surface; PET/CT imaging and with ^{18}F-BG-surface in normal mice; PET/CT imaging of HCCLM3-SNAP tumor-bearing mice with ^{18}F-BG-surface; HRMS of BG-surface-PEG4-p-SCN-Bn-NOTA; and H NMR and C NMR of BG-surface-PEG4-p-SCN-Bn-NOTA (PDF)

■ AUTHOR INFORMATION

Corresponding Authors

Wei Fan − *Department of Nuclear Medicine, Sun Yat-sen University State Key Laboratory of Oncology in South China; Collaborative Innovation Center for Cancer Medicine, Sun Yat-sen University Cancer Center, Guangzhou, Guangdong Province 510060, China*; Email: fanwei@sysucc.org.cn

Guokai Feng − *State Key Laboratory of Oncology in South China; Collaborative Innovation Center for Cancer Medicine, Sun Yat-sen University Cancer Center, Guangzhou, Guangdong Province 510060, China*; orcid.org/0000-0002-8251-291X; Email: fengguok@sysucc.org.cn

Xiaofei Zhang − *Department of Nuclear Medicine, Sun Yat-sen University State Key Laboratory of Oncology in South China; Collaborative Innovation Center for Cancer Medicine, Sun Yat-sen University Cancer Center, Guangzhou, Guangdong Province 510060, China*; orcid.org/0000-0001-9026-0903; Email: zhangxf1@sysucc.org.cn

Authors

Xinling Li − *Department of Nuclear Medicine, Sun Yat-sen University State Key Laboratory of Oncology in South China; Collaborative Innovation Center for Cancer Medicine, Sun Yat-sen University Cancer Center, Guangzhou, Guangdong Province 510060, China*

Xiaochun Yang − *Department of Nuclear Medicine, Sun Yat-sen University State Key Laboratory of Oncology in South China; Collaborative Innovation Center for Cancer Medicine, Sun Yat-sen University Cancer Center, Guangzhou, Guangdong Province 510060, China*

Zhijian Li − *Department of Nuclear Medicine, Sun Yat-sen University State Key Laboratory of Oncology in South China; Collaborative Innovation Center for Cancer Medicine, Sun Yat-sen University Cancer Center, Guangzhou, Guangdong Province 510060, China*

Xiaobin Zheng − *Department of Nuclear Medicine, Sun Yat-sen University State Key Laboratory of Oncology in South China; Collaborative Innovation Center for Cancer Medicine, Sun Yat-sen University Cancer Center, Guangzhou, Guangdong Province 510060, China*

Yong-jian Peng − *State Key Laboratory of Oncology in South China; Collaborative Innovation Center for Cancer Medicine, Sun Yat-sen University Cancer Center, Guangzhou, Guangdong Province 510060, China*

Wenjie Lin − *State Key Laboratory of Oncology in South China; Collaborative Innovation Center for Cancer Medicine, Sun Yat-sen University Cancer Center, Guangzhou, Guangdong Province 510060, China*

Ling Zhou − *Sun Yat-sen University State Key Laboratory of Oncology in South China; Collaborative Innovation Center for Cancer Medicine, Sun Yat-sen University Cancer Center, Guangzhou, Guangdong Province 510060, China*

Dehai Cao − *State Key Laboratory of Oncology in South China; Collaborative Innovation Center for Cancer Medicine, Sun Yat-sen University Cancer Center, Guangzhou, Guangdong Province 510060, China*

Minyi Situ − *State Key Laboratory of Oncology in South China; Collaborative Innovation Center for Cancer Medicine, Sun Yat-sen University Cancer Center, Guangzhou, Guangdong Province 510060, China*

Qingqiang Tu − *Laboratory Animal Center, Sun Yat-sen University Zhongshan School of Medicine, Guangzhou, Guangdong Province 510085, China*

Huiqiang Huang − *State Key Laboratory of Oncology in South China; Collaborative Innovation Center for Cancer Medicine, Sun Yat-sen University Cancer Center, Guangzhou, Guangdong Province 510060, China*

Complete contact information is available at: https://pubs.acs.org/10.1021/acsomega.1c05856

Author Contributions

⊥X.L., X.Y., and Z.L. contributed equally to this work.

Notes

The authors declare no competing financial interest.

■ ACKNOWLEDGMENTS

This work was supported by the National Science & Technology Major Project of China (2017ZX09304021), the National Natural Science Foundation of China (NSFC) (projects 81972531, 82001855, and 82002466), and the Fundamental Research Funds for the Central Universities 19ykpy174. The authenticity of this article has been validated by uploading the key raw data onto the Research Data Deposit public platform (www.researchdata.org.cn) with the approval RDD number as RDDB2022501351.

■ REFERENCES

(1) Volpe, A.; Lang, C.; Lim, L.; Man, F.; Kurtys, E.; Ashmore-Harris, C.; Johnson, P.; Skourti, E.; de Rosales, R. T. M.; Fruhwirth, G. O. Spatiotemporal PET Imaging Reveals Differences in CAR-T Tumor Retention in Triple-Negative Breast Cancer Models. *Mol. Ther.* **2020**, *28*, 2271−2285.

(2) McCutcheon, D. C.; Lee, G.; Carlos, A.; Montgomery, J. E.; Moellering, R. E. Photoproximity Profiling of Protein-Protein Interactions in Cells. *J. Am. Chem. Soc.* **2020**, *142*, 146−153.

(3) Grosser, R.; Cherkassky, L.; Chintala, N.; Adusumilli, P. S. Combination Immunotherapy with CAR T Cells and Checkpoint Blockade for the Treatment of Solid Tumors. *Cancer Cell* **2019**, *36*, 471−482.

(4) Perrin, J.; Capitao, M.; Mougin-Degraef, M.; Guerard, F.; Faivre-Chauvet, A.; Rbah-Vidal, L.; Gaschet, J.; Guilloux, Y.; Kraeber-Bodere, F.; Cherel, M.; et al. Cell Tracking in Cancer Immunotherapy. *Front. Med.* **2020**, *7*, No. 34.

(5) Mowday, A. M.; Copp, J. N.; Syddall, S. P.; Dubois, L. J.; Wang, J.; Lieuwes, N. G.; Biemans, R.; Ashoorzadeh, A.; Abbattista, M. R.; Williams, E. M.; et al. *E. coli* nitroreductase NfsA is a reporter gene for non-invasive PET imaging in cancer gene therapy applications. *Theranostics* **2020**, *10*, 10548−10562.

(6) Wada, A.; Yasumura, S.; Kajikawa, S.; Murakami, J.; Sato, T. Successful treatment of myelomatous pleural effusion with daratu-

mumab administration before autologous peripheral stem cell transplantation. *Rinsho Ketsueki* **2020**, *61*, 879−884.
(7) Huang, C.; Wu, L.; Liu, R.; Li, W.; Li, Z.; Li, J.; Liu, L.; Shan, B. Efficacy and safety of CD19 chimeric antigen receptor T cells in the treatment of 11 patients with relapsed/refractory B-cell lymphoma: a single-center study. *Ann. Transl. Med.* **2020**, *8*, 1048.
(8) Grana, A.; Gut, N.; Williams, K.; Maakaron, J.; Porter, K.; William, B. M.; Vasu, S.; Penza, S.; Brammer, J. E.; Saad, A.; et al. Safety of Axicabtagene Ciloleucel for the Treatment of Relapsed or Refractory Large B-Cell Lymphoma. *Clin. Lymphoma Myeloma Leuk.* **2021**, *21*, 238−245.
(9) Yan, M.; Wu, Y. J.; Chen, F.; Tang, X. W.; Han, Y.; Qiu, H. Y.; Sun, A. N.; Xue, S. L.; Jin, Z. M.; Wang, Y.; et al. CAR T-cell bridging to allo-HSCT for relapsed/refractory B-cell acute lymphoblastic leukemia: the follow-up outcomes. *Zhonghua Xueyexue Zazhi* **2020**, *41*, 710−715.
(10) Ganatra, S.; Redd, R.; Hayek, S. S.; Parikh, R.; Azam, T.; Yanik, G. A.; Spendley, L.; Nikiforow, S.; Jacobson, C.; Nohria, A. Chimeric Antigen Receptor T-Cell Therapy-Associated Cardiomyopathy in Patients With Refractory or Relapsed Non-Hodgkin Lymphoma. *Circulation* **2020**, *142*, 1687−1690.
(11) Schubert, M. L.; Schmitt, M.; Wang, L.; Ramos, C. A.; Jordan, K.; Tidow, C. M.; Dreger, P. Side-effect management of chimeric antigen receptor (CAR) T-cell therapy. *Ann. Oncol.* **2021**, *32*, 34−48.
(12) England, C. G.; Jiang, D.; Ehlerding, E. B.; Rekoske, B. T.; Ellison, P. A.; Hernandez, R.; Barnhart, T. E.; McNeel, D. G.; Huang, P.; Cai, W. (89)Zr-labeled nivolumab for imaging of T-cell infiltration in a humanized murine model of lung cancer. *Eur. J. Nucl. Med. Mol. Imaging* **2018**, *45*, 110−120.
(13) Wei, W.; Jiang, D.; Ehlerding, E. B.; Luo, Q.; Cai, W. Noninvasive PET Imaging of T cells. *Trends Cancer* **2018**, *4*, 359−373.
(14) Wang, X. Y.; Wang, Y.; Wu, Q.; Liu, J. J.; Liu, Y.; Pan, D. H.; Qi, W.; Wang, L. Z.; Yan, J. J.; Xu, Y. P.; et al. Feasibility study of (68)Ga-labeled CAR T cells for in vivo tracking using micro-positron emission tomography imaging. *Acta Pharmacol. Sin.* **2021**, *42*, 824−831.
(15) Sellmyer, M. A.; Richman, S. A.; Lohith, K.; Hou, C.; Weng, C. C.; Mach, R. H.; O'Connor, R. S.; Milone, M. C.; Farwell, M. D. Imaging CAR T Cell Trafficking with eDHFR as a PET Reporter Gene. *Mol. Ther.* **2020**, *28*, 42−51.
(16) Simonetta, F.; Alam, I. S.; Lohmeyer, J. K.; Sahaf, B.; Good, Z.; Chen, W.; Xiao, Z.; Hirai, T.; Scheller, L.; Engels, P.; et al. Molecular Imaging of Chimeric Antigen Receptor T Cells by ICOS-ImmunoPET. *Clin. Cancer Res.* **2021**, *27*, 1058−1068.
(17) Man, F.; Khan, A. A.; Carrascal-Minino, A.; Blower, P. J.; de Rosales, R. T. A kit formulation for the preparation of [(89)Zr]Zr-(oxinate)4 for PET cell tracking: White blood cell labelling and comparison with [(111)In]In(oxinate)3. *Nucl. Med. Biol.* **2020**, *90*−*91*, 31−40.
(18) Moroz, M. A.; Zhang, H.; Lee, J.; Moroz, E.; Zurita, J.; Shenker, L.; Serganova, I.; Blasberg, R.; Ponomarev, V. Comparative Analysis of T Cell Imaging with Human Nuclear Reporter Genes. *J. Nucl. Med.* **2015**, *56*, 1055−1060.
(19) Krebs, S.; Ahad, A.; Carter, L. M.; Eyquem, J.; Brand, C.; Bell, M.; Ponomarev, V.; Reiner, T.; Meares, C. F.; Gottschalk, S.; et al. Antibody with Infinite Affinity for In Vivo Tracking of Genetically Engineered Lymphocytes. *J. Nucl. Med.* **2018**, *59*, 1894−1900.
(20) Heidari, P.; Kunawudhi, A.; Martinez-Quintanilla, J.; Szretter, A.; Shah, K.; Mahmood, U. Somatostatin receptor type 2 as a radiotheranostic PET reporter gene for oncologic interventions. *Theranostics* **2018**, *8*, 3380−3391.
(21) Zhang, H.; Moroz, M. A.; Serganova, I.; Ku, T.; Huang, R.; Vider, J.; Maecke, H. R.; Larson, S. M.; Blasberg, R.; Smith-Jones, P. M. Imaging expression of the human somatostatin receptor subtype-2 reporter gene with 68Ga-DOTATOC. *J. Nucl. Med.* **2011**, *52*, 123−131.
(22) Doubrovin, M. M.; Doubrovina, E. S.; Zanzonico, P.; Sadelain, M.; Larson, S. M.; O'Reilly, R. J. In vivo imaging and quantitation of adoptively transferred human antigen-specific T cells transduced to express a human norepinephrine transporter gene. *Cancer Res.* **2007**, *67*, 11959−11969.
(23) Keu, K. V.; Witney, T. H.; Yaghoubi, S.; Rosenberg, J.; Kurien, A.; Magnusson, R.; Williams, J.; Habte, F.; Wagner, J. R.; Forman, S.; et al. Reporter gene imaging of targeted T cell immunotherapy in recurrent glioma. *Sci. Transl. Med.* **2017**, *9*, No. eaag2196.
(24) Murty, S.; Labanieh, L.; Murty, T.; Gowrishankar, G.; Haywood, T.; Alam, I. S.; Beinat, C.; Robinson, E.; Aalipour, A.; Klysz, D. D.; et al. PET Reporter Gene Imaging and Ganciclovir-Mediated Ablation of Chimeric Antigen Receptor T Cells in Solid Tumors. *Cancer Res.* **2020**, *80*, 4731−4740.
(25) Hussain, A. F.; Heppenstall, P. A.; Kampmeier, F.; Meinhold-Heerlein, I.; Barth, S. One-step site-specific antibody fragment auto-conjugation using SNAP-tag technology. *Nat. Protoc.* **2019**, *14*, 3101−3125.
(26) Campos, C.; Kamiya, M.; Banala, S.; Johnsson, K.; Gonzalez-Gaitan, M. Labelling cell structures and tracking cell lineage in zebrafish using SNAP-tag. *Dev. Dyn.* **2011**, *240*, 820−827.
(27) Depke, D. A.; Konken, C. P.; Rösner, L.; Hermann, S.; Schäfers, M.; Rentmeister, A. A novel 18F-labeled clickable substrate for targeted imaging of SNAP-tag expressing cells by PET in vivo. *Chem. Commun.* **2021**, *57*, 9850−9853.
(28) Laverman, P.; McBride, W. J.; Sharkey, R. M.; Eek, A.; Joosten, L.; Oyen, W. J. G.; Goldenberg, D. M.; Boerman, O. C. A Novel Facile Method of Labeling Octreotide with 18F-Fluorine. *J. Nucl. Med.* **2010**, *51*, 454−461.
(29) McBride, W. J.; D'Souza, C. A.; Sharkey, R. M.; Karacay, H.; Rossi, E. A.; Chang, C.-H.; Goldenberg, D. M. Improved 18F Labeling of Peptides with a Fluoride-Aluminum-Chelate Complex. *Bioconjugate Chem.* **2010**, *21*, 1331−1340.
(30) Kumar, K.; Ghosh, A. 18F-AlF Labeled Peptide and Protein Conjugates as Positron Emission Tomography Imaging Pharmaceuticals. *Bioconjugate Chem.* **2018**, *29*, 953−975.
(31) Nucl, J.; MedBojkowska, K.; Santoni de Sio, F.; Barde, I.; Offner, S.; Verp, S.; Heinis, C.; Johnsson, K.; Trono, D. Measuring in vivo protein half-life. *Chem. Biol.* **2011**, *18*, 805−815.
(32) Dolan, M. E.; Chae, M. Y.; Pegg, A. E.; Mullen, J. H.; Friedman, H. S.; Moschel, R. C. Metabolism of O6-benzylguanine, an inactivator of O6-alkylguanine-DNA alkyltransferase. *Cancer Res.* **1994**, *54*, 5123−5130.
(33) Grant, F. D.; Fahey, F. H.; Packard, A. B.; Davis, R. T.; Alavi, A.; Treves, S. T. Skeletal PET with 18F-Fluoride: Applying New Technology to an Old Tracer. *J. Nucl. Med.* **2008**, *49*, 68.
(34) Minn, I.; Huss David, J.; Ahn, H.-H.; Chinn Tamara, M.; Park, A.; Jones, J.; Brummet, M.; Rowe Steven, P.; Sysa-Shah, P.; Du, Y.; et al. Imaging CAR T cell therapy with PSMA-targeted positron emission tomography. *Sci. Adv.* **2019**, *5*, No. eaaw5096.

https://doi.org/10.1021/acsomega.1c05856
ACS Omega 2022, 7, 7550−7555